

Understanding the Surface Structure and Catalytic Activity of SnO_x/Au(111) Inverse Catalysts for CO₂ and H₂ Activation

J. Kang, J. A. Rodriguez

To be published in "Journal of Physical Chemistry C"

March 2022

Chemistry Department
Brookhaven National Laboratory

U.S. Department of Energy
USDOE Office of Science (SC), Basic Energy Sciences (BES) (SC-22)

Notice: This manuscript has been authored by employees of Brookhaven Science Associates, LLC under Contract No. DE-SC0012704 with the U.S. Department of Energy. The publisher by accepting the manuscript for publication acknowledges that the United States Government retains a non-exclusive, paid-up, irrevocable, world-wide license to publish or reproduce the published form of this manuscript, or allow others to do so, for United States Government purposes.

DISCLAIMER

This report was prepared as an account of work sponsored by an agency of the United States Government. Neither the United States Government nor any agency thereof, nor any of their employees, nor any of their contractors, subcontractors, or their employees, makes any warranty, express or implied, or assumes any legal liability or responsibility for the accuracy, completeness, or any third party's use or the results of such use of any information, apparatus, product, or process disclosed, or represents that its use would not infringe privately owned rights. Reference herein to any specific commercial product, process, or service by trade name, trademark, manufacturer, or otherwise, does not necessarily constitute or imply its endorsement, recommendation, or favoring by the United States Government or any agency thereof or its contractors or subcontractors. The views and opinions of authors expressed herein do not necessarily state or reflect those of the United States Government or any agency thereof.

Understanding the Surface Structure and Catalytic Activity of SnO_x/Au(111) Inverse Catalysts for CO₂ and H₂ Activation

Jindong Kang,^{1†} Ning Rui,^{2†} Rina Rosales,¹ Yi Tian,¹ Sanjaya D. Senanayake,² and José A. Rodríguez^{1,2*}

¹ Department of Chemistry, SUNY at Stony Brook, Stony Brook, NY, 11794 USA

² Chemistry Department, Brookhaven National Laboratory, Upton, NY, 11973 USA

* Corresponding author, E-mail: rodriguez@bnl.gov

Abstract

Carbon dioxide hydrogenation is a promising approach for the reduction of greenhouse gas pollution via the production of fuels and high value chemicals utilizing C1 chemistry. In this process, the activation of non-polar molecules, CO₂ and H₂, at mild conditions is challenging. Herein, we report a well-defined inverse SnO_x/Au(111) catalyst that shows ability to activate both CO₂ and H₂ at room temperature. Scanning tunneling microscopy (STM) and ambient pressure X-ray photoemission spectroscopy (AP-XPS) are combined to understand the surface structure, growth mode, chemical state, and activity of SnO_x/Au(111) surfaces. Nanostructures of SnO_x at a sub-monolayer level were prepared by depositing Sn on Au(111) followed by O₂ oxidation. For the as-prepared SnO_x/Au(111), two-dimensionally formed SnO_x thin film on Au(111) substrate were observed with STM of two different moieties, discernable based on their height: clusters (~ 0.4 Å) and nanoparticles (NPs, 1 – 2.5 Å), which are assigned to Sn-Au alloys and SnO_x, respectively, in corroboration with XPS analysis. Furthermore, SnO_x/Au(111) was annealed under UHV to test its thermal stability. Upon annealing at 400 - 600 K, a disappearance of SnO_x NPs and re-appearance of highly dispersed Sn clusters was clearly noticeable from the STM and XPS results, identifying the thermal decomposition of SnO_x and subsequent formation of Sn-Au alloys on the surface due to the recombination of Sn clusters with Au. We investigated the reactivity of the SnO_x/Au(111) surfaces towards CH₄, CO₂ and H₂. The SnO_x/Au(111) surfaces have excellent CO₂ and H₂ activation ability even at room temperature with negligible reactivity for methane activation. Our AP-XPS results show that H₂ can be activated on the SnO_x NPs by the reduction to Sn. For CO₂, the activation and further dissociation is identified by a re-oxidation of Sn with newly formed Sn-O bonds, and the formation of surface carbon. Therefore, we propose that SnO_x is a potential catalyst or additive to achieve CO₂ hydrogenation under mild conditions.

Introduction

CO₂ and CH₄ are major greenhouse gases generated by human activities.¹⁻³ In principle, the chemical recycling of CO₂ or CH₄ can provide a renewable, carbon-neutral, unlimited source for the reduction of atmospheric pollutants and production of fuels and high value chemicals.⁴ Since CO₂ and CH₄ are highly stable and non-polar molecules, their conversion usually requires the use of catalysts, which must be able to adsorb and activate CO₂ or CH₄ efficiently.^{2,5-8} Most of the catalysts used in the industry involve metal nanoparticles supported on an oxide substrate.⁵⁻⁷ Usually, moderate or high temperatures are required as energy to enable the CO₂ or CH₄ conversion.⁹

The concept of a system composed of a metal oxide deposited on a plain metal support, also known as inverse oxide/metal catalysts, is often used to explore or utilize the synergistic effect of metal-metal oxide interface sites towards enhanced catalytic activity.¹⁰⁻¹³ Oxide nanoparticles or monolayer thin films, when placed on metal supports, show unique physical, chemical, and electronic properties when compared to their bulk counterparts.¹³⁻¹⁵ This is because their small size can lead to quantum effects, and also the nanoparticles typically can have a high density of defects, corner or edge surface sites.¹³⁻¹⁵ Lunkenbein *et al.* observed the formation of zinc oxide overlayers on top of copper particles in powder Cu/ZnO/Al₂O₃ catalysts used for industrial methanol synthesis under reaction conditions.¹⁶ The active phase, ZnO_x overlayers, turned out to be a graphite-like structure which is different from the stable wurtzite structure typically seen for bulk ZnO.¹⁶ In fact, the ZnO/Cu inverse system demonstrated an enhanced catalytic activity when compared to a catalyst with a conventional Cu/ZnO configuration.¹⁷ Furthermore, a small fraction of ceria (CeO_x) or titania (TiO_x) deposited on a Au support revealed excellent activity toward the water-gas shift reaction

(WGS), even showing comparable or better performance than Cu(111) or Cu(100), the benchmark catalyst for the WGS process; whereas neither bulk Au nor bulk ceria and titania show significant activity.¹⁸

These phenomena or trends originate in strong oxide-metal interactions caused by the special physical and chemical properties of the oxide structures on top of a metal substrate that also can participate in the catalytic process.^{10–15} This is in contrast to oxides in many industrial catalysts which are employed simply as high surface area supports for the dispersion of metal particles.^{19–21} Moreover, inverse model catalysts offer an advantage for understanding the role of the oxide component in a catalytic process; whereas the complexity and heterogeneity of powder catalysts make it difficult to obtain fundamental insight of their catalytic activities.^{22–24} In this context, we applied the inverse configuration to investigate the structure and catalytic properties of tin oxide (SnO_x) on an well-defined substrate, Au(111) single crystal.

Sn and SnO_x have been studied and employed in the past for gas sensors^{25–28} and used in diverse types of catalytic reactions such as ethanol oxidation for fuel cells, CO oxidation, electrochemical CO_2 reduction, dry reforming and steam reforming of methane, partial oxidation of methane, and methane chlorination.^{29–34} Additionally, in a previous study, our group investigated methane activation on highly dispersed SnO_x NPs that were grown on $\text{Cu}_2\text{O}/\text{Cu}(111)$ using reactive deposition.³⁵ This study demonstrated that $\text{SnO}_x/\text{CuO}_x/\text{Cu}(111)$ catalysts activate methane even at room temperature and enhance the activity upon creation of a $\text{SnO}_x\text{-Cu}_2\text{O}$ interface.³⁵ However, the contribution of pure SnO_x without any interfacial sites cannot be distinguished by such a system, due to the existence of an active $\text{SnO}_x\text{-Cu}_2\text{O}$ interface. Thus, for academic and practical reasons, it is important to establish the intrinsic reactivity of SnO_x NPs towards typical reactant molecules used in the conversion of CO_2 or CH_4 .

In the present study, we used a well-defined Au(111) as a substrate, which is well known to be inert in various reactions.^{18,36,37} Sub-monolayers of SnO_x were prepared by vapor-depositing Sn on Au(111) followed by oxidation at room temperature. Thus, the intrinsic property of SnO_x NPs can be studied without any interaction with the substrate. By means of scanning tunneling microscopy (STM) and ambient pressure X-ray photoelectron spectroscopy (AP-XPS), we performed a series of experiments to obtain the morphology of the SnO_x NPs and to test their ability to activate molecules frequently used in C1 chemistry (CO₂, CH₄, and H₂).

Experimental Methods:

All the STM experiments were conducted using an Omicron STM instrument housed in an ultra-high vacuum chamber with a background pressure of 9×10^{-10} Torr. A Au(111) single crystal (Princeton Scientific Corp) was cleaned by cycles of Ar ion sputtering (2 kV, 15 min) and annealing (650 K, 20min). The STM images were collected at room temperature by using a Pt–Ir tip. Tin was vapor-deposited at room temperature on the clean Au(111) surface. SnO_x overlayers were subsequently prepared by exposing 50 mTorr of oxygen for 30 min in a high-pressure cell at room temperature. For thermal stability test, as prepared SnO_x/Au(111) surfaces were annealed to 400, 500, and 600 K, consecutively. The preparation methods for our SnO_x films on the Au single crystal surface were adopted and modified from those of our previously reported study for ZnO films, which provided the known inverse ZnO/Cu configuration for methanol synthesis.^{38,39} In our STM studies, the coverages of Sn or SnO_x features were determined with a program by calculating the area of protruding or depressed features relative to the Au surface, and the calculated coverages were obtained from comparing

and taking average of more than 50 different large areas.

Ambient pressure XPS (AP-XPS) experiments were conducted using an instrument available at the Chemistry Department of Brookhaven National Laboratory (BNL). A commercial SPECS AP-XPS chamber equipped with a PHOIBOS 150 EP MCD-9 analyzer and a Mg K α anode was used to record the Au 4f, Sn 3d, O 1s, and C 1s regions. A Au(111) single crystal, cleaned by cycles of Ar ion sputtering and annealing (800 K, 10 min), was used as a substrate to grow SnO_x overlayers. Nanoclusters of SnO_x were deposited following the same methodology applied to the STM experiments described above. The CH₄, CO₂ and H₂ activation were studied at temperatures in the range between 300 and 500 K. Following the initial characterization in the UHV chamber, a reaction feed of H₂ (20 mTorr) or CO₂ (50 mTorr) was introduced sequentially to the SnO_x/Au(111) surfaces, and finally the samples were rapidly heated to the desired reaction temperature.

Results and Discussion

A. Sn Deposition on Au(111) at Room Temperature: STM studies

It is known that bulk Au and bulk Sn can form different types of alloys.^{40,41} The two metals have a high miscibility even below room temperature. Several studies have reported that Sn deposition on Au(111) forms surface alloys with AuSn and Au₂Sn composition, depending on the substrate temperature.⁴⁰⁻⁴⁴ AES, LEED, XPS and STM investigations revealed two dimensional layer growth of Sn-Au surface alloy with 1:1 ratio of Sn to Au when Sn is deposited on Au at room temperature.^{40,41,44} DFT calculations also found a surface reconstruction and alloy formation by the interaction between the adsorbed Sn ($\theta_{\text{Sn}} = 0.5$ ML) and the 1st and 2nd layers of the gold substrate at room temperature.⁴³ Barthès *et al.* discovered

that rapid diffusion of gold through tin layers occurs at room temperature so that only the alloy structure is observed.⁴¹ Taking into account the larger diffusion coefficient of Au in Sn ($10^{-13} - 10^{-15} \text{ m}^2/\text{s}$) than that of Sn in Au ($10^{-25} \text{ m}^2/\text{s}$)⁴⁵, it seems a valid statement. Similarly, as an evidence of the high miscibility between Sn and Au, we observed a STM tip induced – dynamic formation of Sn-Au surface alloy (Figure S1) and surface reconstruction at room temperature over a long period of time after deposition of a large amount of Sn, which was enough to form multilayers of Sn. Considering the corresponding bond dissociation energies, it is also valid to observe the formation of Sn-Au alloy because the bond energy of Sn-Au (256 kJ/mol) is larger than those of Sn-Sn (187 kJ/mol) and Au-Au(226 kJ/mol).⁴⁶

Figure 1 shows a set of STM images collected before (a) and after (b and c) the deposition of Sn on Au(111) at room temperature. A clean Au(111) surface with the typical herringbone structure is shown in Figure 1a. Figure 1b and 1c represent 0.1 ML Sn on Au(111). The Sn-related nanoclusters appear as depression and are located dominantly around the herringbone elbows. Such depression features are attributed to the incorporation of Sn atoms in the Au surface, and the same phenomena were observed in other surface alloy systems at sub-monolayer coverage levels such as Rh/Au(111), Mn/Au(111), Ni/Au(111), and Co/Cu(001), where there was incorporation of the admetal into the host substrate due to alloying.⁴⁷⁻⁵⁰ The

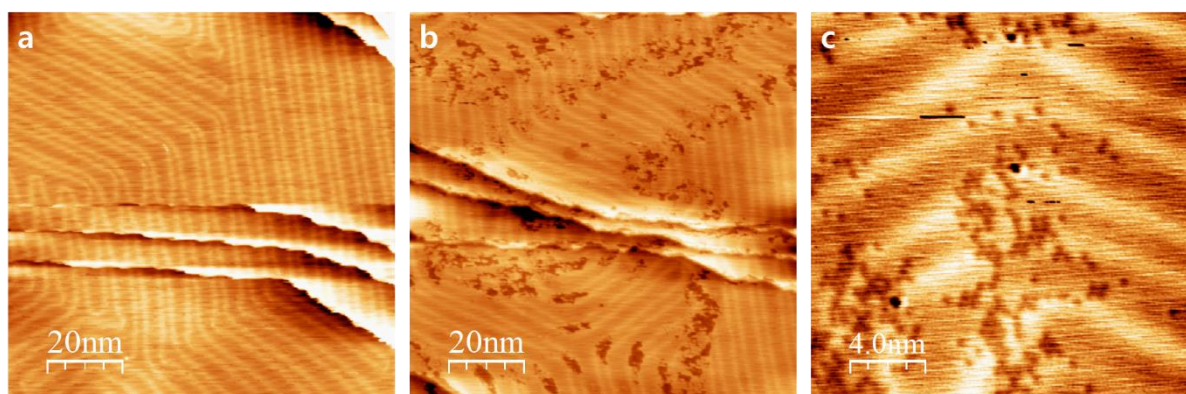


Figure 1. STM images of Au(111) and Sn/Au(111). (a) A clean Au(111) (b) 0.1 ML Sn on Au(111) (c) A zoomed-in region of 0.1 ML Sn/Au(111). Scanning condition: (a) -1.2 V, 0.1 nA, (b) - 0.7 V, 0.14 nA, (c) -0.7 V, 0.12 nA

depth of these depressions in Figure 1 is in the range of 0.25 – 0.5 Å, and this agrees with the reported value by Sadhukhan *et al* for 0.01ML of Sn on Au(111).⁴⁰ Increasing the admetal coverage, a surface with 0.3 ML of Sn on Au(111) was prepared and shown in Figure S2. Due to the lower surface free energy of Sn ($\sim 0.7 \text{ J/m}^2$) compared to that of Au ($\sim 1.5 \text{ J/m}^2$),⁵¹ we observed surface wetting of Sn on Au(111), connecting the thin Sn domains localized at each elbow site along the $\langle 112 \rangle$ direction, instead of the formation of three-dimensional island of Sn.

B. Oxidation of Sn/Au(111) by O₂ at Room Temperature: STM studies

The formation of SnO₂ is a highly exothermic reaction ($\Delta H_{298\text{K}}^{\circ} = -578 \text{ kJ/mol}$), but the oxidation of metallic tin can be retarded by kinetic effects.^{25,26} When a 0.1 ML Sn/Au(111) surface was exposed to O₂ with a pressure of 50 mTorr for 30 minutes, bright nanoparticles appear at the elbow sites and step edge (Figure 2). There are two types of species found in Figure 2a according to their height: Clusters ($\sim 0.4 \text{ \AA}$) and nanoparticles ($\sim 2 \text{ \AA}$). The line profiles 1 and 2 in Figure 2b were measured on clusters and a nanoparticle, respectively, as examples. The height of the clusters is comparable to the depth of Sn on Au(111) in Figure 1c, and these clusters are considered to be the remaining Sn-Au surface alloys even after 30 minutes oxidation with 50 mTorr of O₂. Meanwhile, the bright protruded particles are likely ascribed to SnO_x. The presence of both a Sn-Au alloy and SnO_x on this surface was further confirmed by the XPS results which will be discussed in detail in the following section. While Figure 2 shows only protruded features, Figure S3 obtained by applying different polarity on the tip shows both depression and protrusion features on the surface and indicates the mixed states of the deposited Sn. The depression features are likely attributed to a Sn-Au alloy, which are also found in Figure 1b and 1c, and the bright protruded

particles near the elbow sites are likely ascribed to SnO_x formed by pulling out the embedded Sn atoms from the Sn-Au surface alloy via reaction with O_2 . Since the Sn-O bond energy (528

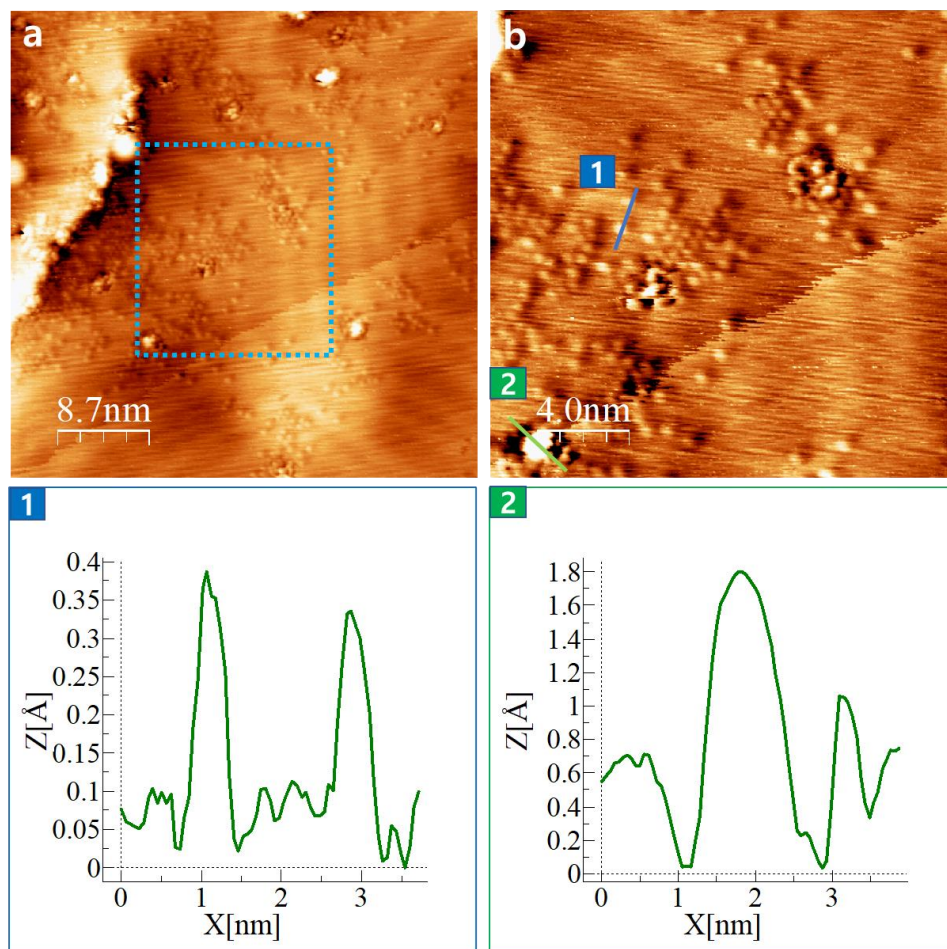


Figure 2. STM images of 0.1 ML $\text{SnO}_x/\text{Au}(111)$. (a) $43 \times 43 \text{ nm}^2$ (b) $20 \times 20 \text{ nm}^2$, blue rectangle region in Figure 2(a). Profile 1 and 2 correspond to SnO_x nanoclusters and nanoparticles in Figure 2(b), respectively. Scanning condition: -0.77V , 0.12nA

kJ/mol) is greater than the Sn-Au bond energy (256 kJ/mol), it is reasonable to observe the formation of SnO_x from the Sn-Au surface alloy upon O_2 oxidation.⁴⁶

To understand the growth behavior of SnO_x , a higher coverage of SnO_x was prepared by increasing the Sn evaporation time. Figure 3 represents different regions of a 0.3 ML $\text{SnO}_x/\text{Au}(111)$ surface. At this coverage, the number of SnO_x nanoparticles has noticeably

increased and many of them are found near step edges as seen in Figure 3b (white circle). The height of these particles is in the range of 1 – 2.5 Å. Since our SnO_x/Au(111) sample was prepared by oxidizing pre-deposited Sn on Au(111), which grows preferentially from the elbows and expands two dimensionally while connecting the elbows, SnO_x appeared as thin films on Au(111) with an average height of 0.6 Å (See Figure 3, line profile 2). Interestingly, the larger SnO_x nanoparticles formed by oxidation were also mostly observed near the herringbone elbow sites on the terrace (Figure 3c), similar to those of the 0.1 ML sample.

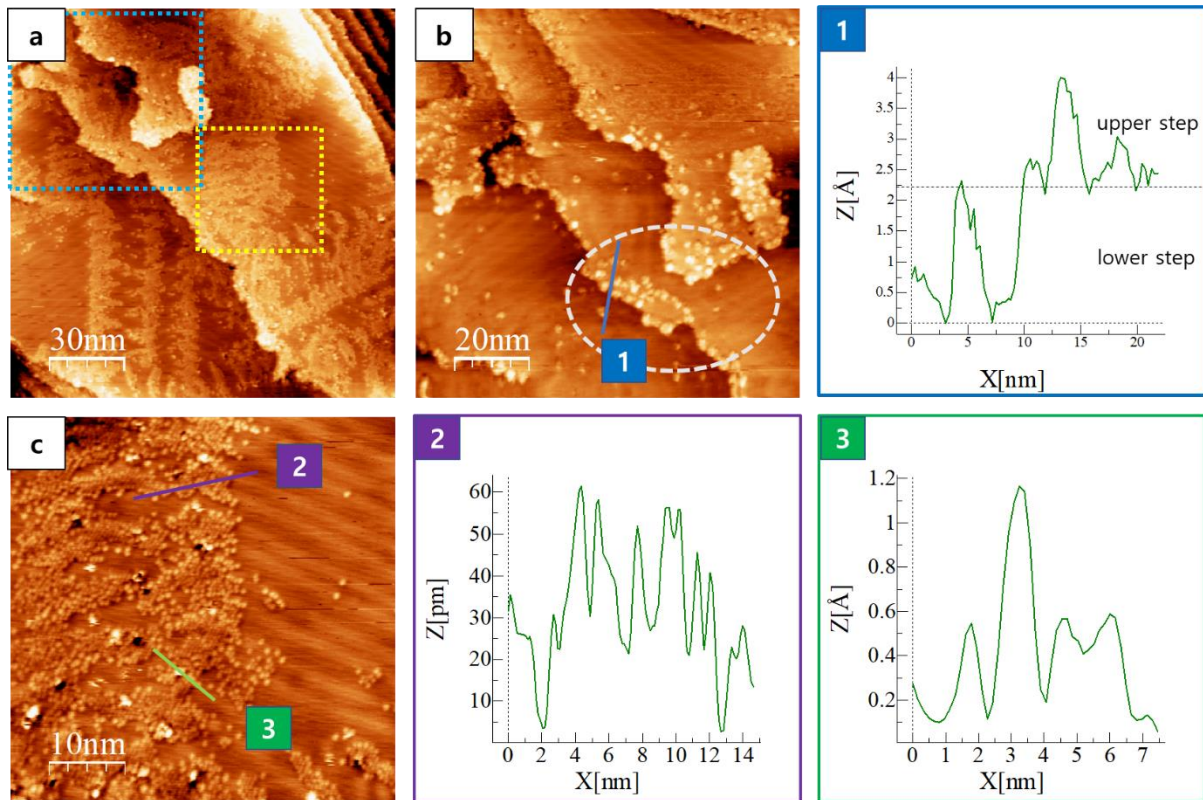


Figure 3. STM images of 0.3 ML SnO_x/Au(111). (a) 150 x 150 nm², (b) 100 x 100 nm², blue rectangle region in Figure 3(a), (c) 50 x 50 nm², yellow rectangle region in Figure 3(a). Profile 1, 2, and 3 correspond to SnO_x nanoparticles and island in Figure 3(b, c). Scanning condition: (a) -1.1 V, 0.1 nA, (b, c) -1.8 V, 0.1 nA.

C. Surface Chemical States of Sn-Au(111) and SnO_x/Au(111): XPS studies

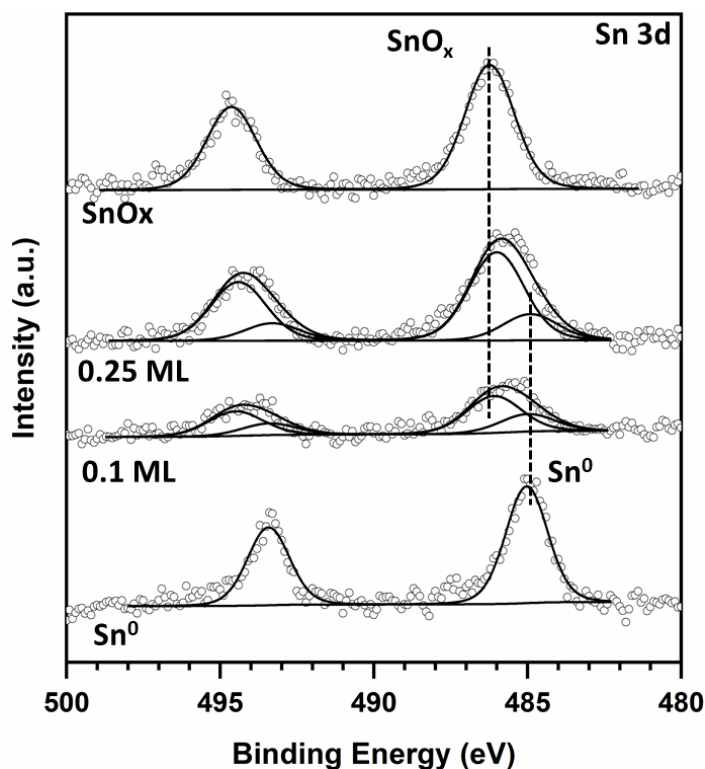


Figure 4. Sn 3d XPS spectra of Sn-Au(111) alloy, a SnO_x film, and pristine SnO_x/Au(111) systems with different coverages. The SnO_x coverages in the samples were estimated to be 0.1 and 0.25 ML as indicated.

XPS was used to probe the chemical state of as-prepared samples, as shown in Figure 4. In this figure, the bottom spectrum, Sn⁰ features,³⁵ is prepared by vapor deposition onto Au(111) substrate without any background O₂ present. Thus, the generated Sn is in a metallic state. This is further confirmed by its binding energy, which is 485.0 eV, consistent with reported value for metallic Sn.³⁵ The top spectrum, SnO_x sample, is prepared by the oxidation of the as-deposited Sn/Au sample at 500 K with 10 mTorr O₂. The binding energy is 486.2 eV, which is 0.5 eV lower than that of reported bulk SnO₂.^{52,53} We also estimated the atomic O/Sn ratio by using the Scofield Relative Sensitivity Factor, which is calculated as 1.3. These results indicate that SnO_x is stabilized on Au(111) as the reduced form compared to bulk SnO₂. Similar stabilization were reported for reduced SnO_x on a Pt(111) surface, as well as reduced TiO_x and

CeO_x islands deposited on a Au(111) substrate.^{18,54} Furthermore, due to the rich electron density on the metal support,^{18,19} electrons may be flowing from the Au(111) surface into the tin oxide overlayer leading to a lower oxidation state in the Sn cations and a lower binding energy with respect to Sn⁴⁺. Interestingly, in our previous work, with a similar deposition method but using pre-oxidized Cu₂O/Cu(111) as the substrate, we were able to fully oxidize the tin, forming SnO₂/Cu₂O/Cu(111). This comparison shows the importance of the substrate and how it can affect the chemical state of deposited tin oxide.

For the 0.1 and 0.25 ML samples, they were prepared by the oxidation of an as-deposited Sn-Au(111) alloy at room temperature to get identical systems to those investigated by STM. It is clearly seen that they consist of both SnO_x and Sn⁰. The atomic fraction of SnO_x increases from 68% to 77% with increasing coverage. The behavior is consistent with the STM images in Figure 3 where more SnO_x NPs are detected in the higher coverage sample. The increase in the amount of SnO_x is correlated with the increasing amount of the deposited Sn species, which was also observed in a previous work for the SnO_x/Pt(111) system.⁵⁵ In addition, XPS showed no evidence of Au oxidation under all tested conditions.

D. Temperature effect on the morphology and chemical state of SnO_x/Au(111)

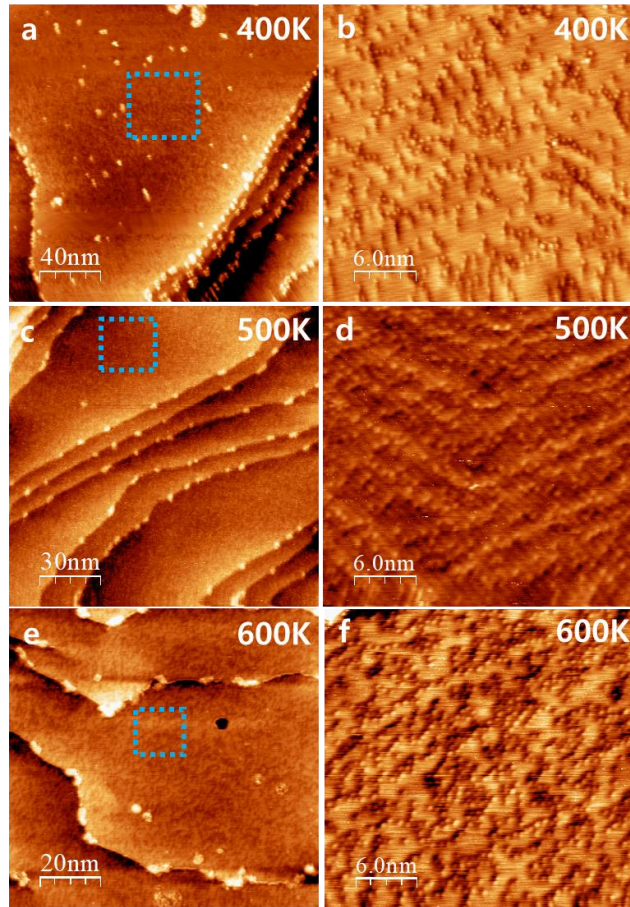


Figure 5. STM images for 0.3 ML SnO_x/Au(111) after UHV annealing to (a, b) 400 K, (c, d) 500 K, (e, f) 600 K. Figure 5 (b, d, f) corresponds to the blue rectangle regions in Figure 5 (a, c, e), respectively.

To investigate the temperature effect on SnO_x, we applied heat to our 0.3 ML SnO_x/Au(111) sample and probed its morphology at room temperature after annealing to 400, 500, and 600 K, as displayed in Figure 5. It was noticeable that the SnO_x thin films observed in Figure 3 were not seen after applying heat. Instead, highly dispersed clusters were observed across the terraces and no longer showed the preferential sites at elbows. At 400 K (Figure 5a), bright nanoparticles still existed on the terraces while they were hardly found on terraces at 500 and 600 K but mostly found at step edges (Figure 5b and 5c). This phenomenon is attributed to the decomposition of SnO_x upon annealing, and subsequent formation of a Sn-Au

alloys with evolution of O_2 gas was expected. Yan *et al.* also reported after reduction via STM the surface morphology of their $SnO_x/Au(111)$ were smoothed as a consequence of instant Sn incorporation to Au.⁵⁶ The XPS results in Figure 6 point to the re-appearance of metallic Sn on the surface as a consequence of annealing.

For the comparison with the result obtained from STM, we also performed annealing experiments with XPS under UHV conditions. As we mentioned, in Figure 5, once the sample is heated to 400 K, we saw the disappearance of SnO_x NPs, and the formation of more Sn clusters, which indicates the thermal decomposition of SnO_x to a Sn-Au alloy. Accordingly, in

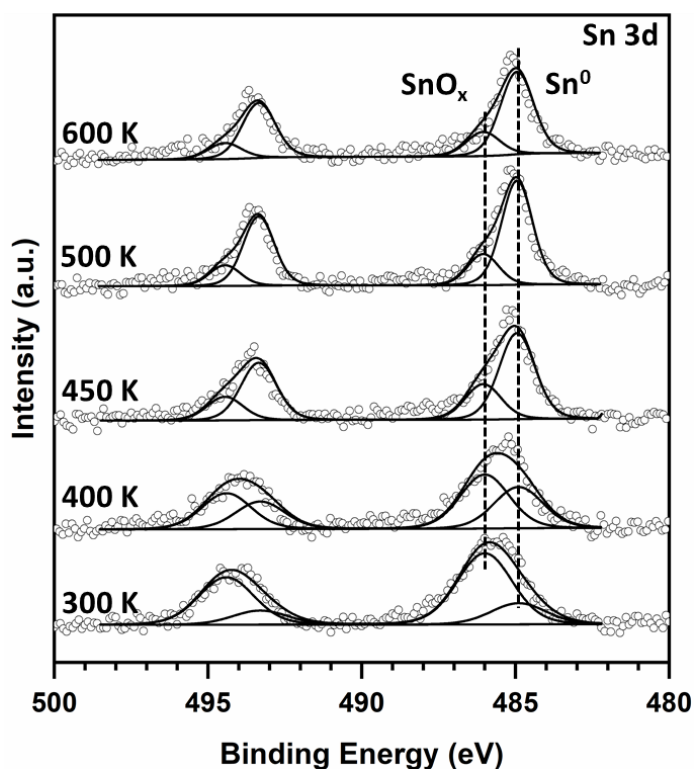


Figure 6. Sn 3d XPS region for a $SnO_x/Cu(111)$ surface ($\theta_{SnO_2} \sim 0.25$ ML) when annealing under UHV at different temperatures.

the XPS spectra displayed in Figure 6, we also see the reduction of SnO_x (486.2 eV) to Sn (485.0 eV). The composition of all samples was fitted with two components, SnO_x (486.2 eV) and Sn (485.0 eV), and was further quantified by the area fraction. Initially at 300 K, about 23%

of Sn⁰ is present in the pristine sample. Once it is annealed to 400 K, the percentage of Sn⁰ is increased to 43%. The reduction becomes more predominant at temperatures above 450 K. Therefore, with increasing annealing temperature, the SnO_x is thermally decomposed into metallic Sn and re-dispersed on the Au(111) surface, as observed in the corresponding STM images. This can be linked to the bond energy of Sn-Au (256 kJ/mol), which is significantly greater than that of Sn-Sn bond (187 kJ/mol)) and Au-Au bond (226 kJ/mol).⁴⁶ When extra energy is applied from heat, the Sn-O bond is cleaved to liberate O and recombine Sn-Au bonds. Hence, we see a clear trend of SnO_x decomposition and re-dispersion in the annealing process.

E. Reactivity of SnO_x/Au(111): Interaction with CH₄, H₂ and CO₂

In the enzyme methane monooxygenase, the conversion of methane into methanol takes place at room temperature and is carried out by a group of three copper cations that can easily activate C-H bonds.^{57,58} The CuO_x/Cu(111) substrate is not efficient for the activation of methane but its reactivity can be enhanced by the addition of NPs of a second oxide.³⁵ Our group at BNL has previously reported that SnO_x/Cu₂O/Cu(111) surfaces can activate methane at room temperature. The CH₄ activation energy is as low as 18.45 kcal mol⁻¹, in sharp contrast with the CH₄ activation energy of 36.90 kcal mol⁻¹ on a bare and perfect Cu₂O/Cu(111) surface.³⁵ Therefore, we first tried CH₄ activation on the SnO_x/Au(111) system. The plain Au(111) surface is inert for this reaction. With this in mind, we can say that any reaction on this system can be attributed mainly to the supported SnO_x alone. Interestingly, the SnO_x/Au(111) surfaces did not show any signs of C-H bond cleavage and the adsorption of CH_x groups. . This result highlights the importance of the SnO_x-CuO_x interface: Only when such interface exists, does the system shows activity towards methane dissociation whereas the

bare Cu₂O/Cu(111) and SnO_x/Au(111) samples do not show significant methane activation.

SnO₂ is widely used as a H₂ sensor.^{25,26,59} Therefore, we introduced 20 mTorr of H₂ into the chamber at room temperature to observe the interaction of H₂ with the SnO_x/Au(111) system. As shown in Figure 7(a), the introduction of H₂ leads to immediate partial reduction of SnO_x to metallic Sn at room temperature. Accordingly, the corresponding O 1s spectrum in Figure 7(b) also shows an attenuation of the total oxygen content.

With this reduced sample, we then evacuated H₂ and dosed 50 mTorr of CO₂ at room temperature. Surprisingly, around 24.3% of the Sn could be re-oxidized to SnO_x also at room

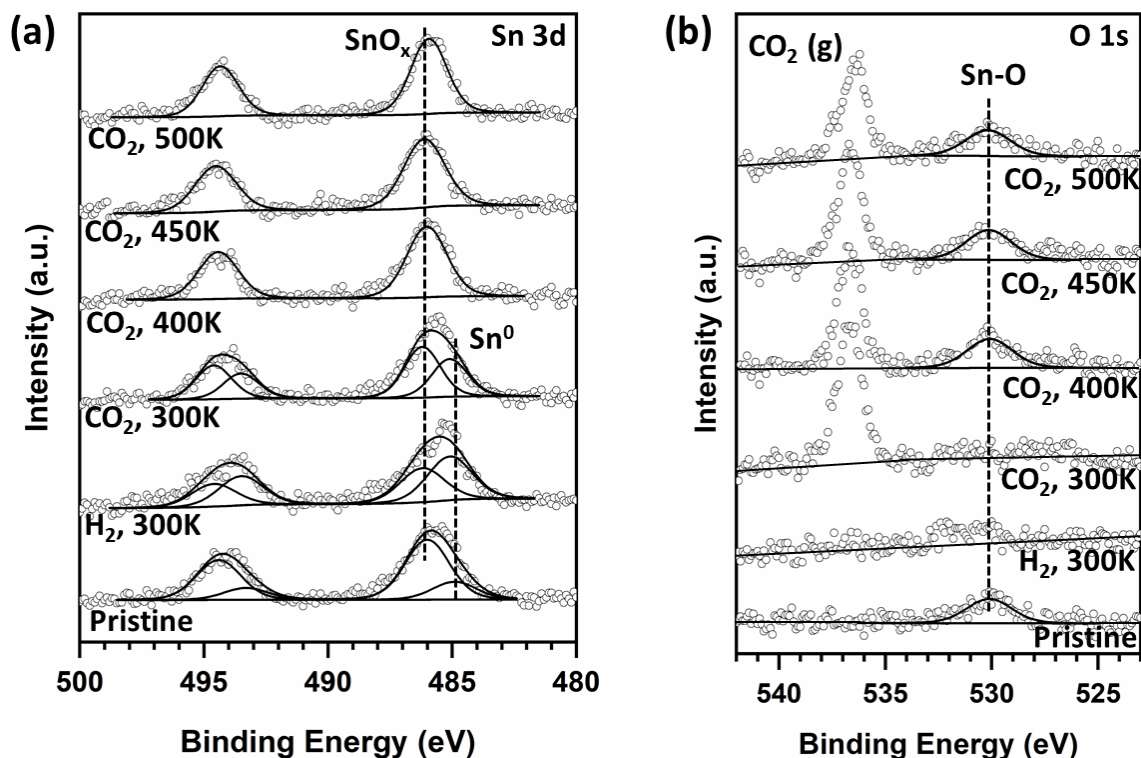
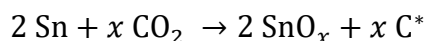


Figure 7. (a) Sn 3d and (b) O 1s regions in AP-XPS spectra for a SnO_x/Au(111) surface ($\theta_{\text{SnO}_2} \sim 0.25$ ML) when exposed to 20 mTorr of H₂ or 50 mTorr of CO₂ at different temperatures.

temperature. If the sample is heated to 400 K or higher, all metallic Sn is re-oxidized and shows a Sn-O bond at 530.1 eV in the O 1s spectra. Figure S4 shows the C 1s XPS spectra collected while exposing the reduced SnO_x/Au(111) sample to CO₂. It is important to note that under

CO₂ ambient, no features are seen for adsorbed CO₂ or carbonate species, only a C* peak is seen near 284.3 eV at 300 and 400 K, at which temperature the sample starts to be re-oxidized. This is a strong indication of the full CO₂ dissociation on the SnO_x nanoparticles:



In our experiments, it was impossible to rule out the desorption of CO formed by the partial decomposition of CO₂. At 300-500 K, this molecule could desorb as soon as it is formed. In any case, the significant amounts of C and O deposited on the surface point to a full decomposition of CO₂. Thus, we highlight that the SnO_x/Au(111) surface is reactive for both H₂ and CO₂ activation at mild conditions, showing great potential to be used as a system for CO₂ hydrogenation. As mentioned above, Au(111) does not activate CO₂. Cu(111), a typical benchmark in studies for CO₂ hydrogenation, is also no good for the activation of carbon dioxide.^{60,61} The SnO_x/Au(111) system displays an activity for the cleavage of C-O bonds that is much larger than that of Au(111) and Cu(111). In principle, SnO_x NPs could be used in novel inverse oxide/metal catalysts or added to existing metal/oxide catalysts to enhance activity for CO₂ hydrogenation.

Since Au(111) is inert, it probably did not have a direct participation in the dissociation of H₂ or CO₂. However, it is a metal substrate with a large electron density that in part could be transferred to the tin oxide overlayer.^{18,19,62} A metal → oxide charge transfer is consistent with the results of XPS in Figure 4 and will reduce the positive charge on the tin cations making them more reactivity than in bulk SnO₂. From previous experimental and theoretical works, it is known that Au(111) enhances the chemical reactivity of CeO₂ and TiO₂ overlayers by increasing the relative stability of the Ce³⁺ and Ti³⁺ states.^{18,19,62} A similar phenomenon could be happening for the Sn³⁺ or Sn²⁺ states in the SnO_x/Au(111) system.

Conclusions

We have investigated the morphology and chemical state of sub-monolayers of tin oxide (SnO_x) grown on a Au(111) substrate by using STM and AP-XPS. To prepare SnO_x , metallic Sn was initially vapor-deposited on Au(111) at room temperature followed by oxidation via 50 mTorr of O_2 . Sn/Au(111) system was also compared with SnO_x /Au(111). We have observed the formation of Sn-Au surface alloys and Sn incorporation into Au near the herringbone elbow sites on the reconstructed Au(111) surface. Due to the strong bond between Sn and Au, two-dimensional growth of Sn on Au (surface wetting) upon increasing the Sn coverage was noticeable from the STM images. The oxidation process resulted in SnO_x nanoparticle formation at both herringbone elbows and step edges, pulling out the embedded Sn from Au to the surface, and the height of particles varied from 1 to 2.5 Å. We have confirmed the presence of both Sn^0 and SnO_x in our oxide samples through XPS and also noticed reduction of SnO_x upon UHV annealing, transitioning from SnO_x to Sn^0 in the temperate range of 300 – 600 K. The STM data with UHV annealing of the surface was consistent with that of the XPS data: A majority of the SnO_x nanoparticles disappeared on the terrace regions and only remained at step edges while highly dispersed Sn clusters were detected on the terraces, recombining with Au.

To investigate the potential catalytic chemistry of the SnO_x NPs, the sample was treated with CH_4 or H_2 and CO_2 sequentially. There was no activation of methane on the SnO_x /Au(111) surfaces. This was in contrast to the behavior seen previously for SnO_x /CuO_x/Cu(111). The lack of a SnO_x -CuO_x interface made impossible the activation of methane. On the other hand, the supported SnO_x NPs alone were very effective for H_2 and CO_2 activation, accompanied by

redox chemistry under mild conditions. At 300 K, H₂ was activated on the surface and then reduced the SnO_x to Sn. Upon exposure to CO₂, the molecule fully decomposed to re-oxidize the SnO_x and formed carbon species on the SnO_x/Au(111) surface. These findings point to a great potential for the use of SnO_x NPs in catalyst for CO₂ hydrogenation.

Supporting Information

STM Images of surface reconstruction of Sn/Au(111) upon tip-induced dynamic formation of Sn-Au alloy; STM Images of 0.1 and 0.3 ML SnO_x/Au(111); C 1s regions in AP-XPS spectra for the SnO_x/Au(111) surface ($\theta_{\text{SnO}_2} \sim 0.25$ ML) when exposed to 20 mTorr of H₂ or 50 mTorr of CO₂ at different temperatures.

Acknowledgement

The research was carried out at Brookhaven National Laboratory (BNL) and supported by the division of Chemical Science, Geoscience, and Bioscience, Office of Basic Energy Science of the US Department of Energy (DOE) under Contract No. DE-SC0012704.

References

- (1) Olah, G. A.; Prakash, G. K. S.; Goepfert, A. Anthropogenic Chemical Carbon Cycle for a Sustainable Future. *J. Am. Chem. Soc.* **2011**, *133*, 12881–12898.
- (2) Orozco, I.; Huang, E.; Mahapatra, M.; Kang, J.; Shi, R.; Nemšák, S.; Tong, X.; Senanayake, S. D.; Liu, P.; Rodríguez, J. A. Understanding Methanol Synthesis on Inverse ZnO/CuO_x/Cu Catalysts: Stability of CH₃O Species and Dynamic Nature of the Surface. *J. Phys. Chem. C* **2021**, *125*, 6673–6683.
- (3) Nisbet, E. G.; Dlugokencky, E. J.; Bousquet, P. Methane on the Rise-Again. *Science*. **2014**, *343*, 493–495.
- (4) Olah, G. A. Beyond Oil and Gas: The Methanol Economy. *Angew. Chemie - Int. Ed.* **2005**, *44*, 2636–

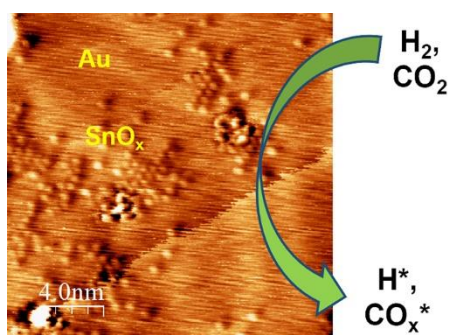
2639.

- (5) Graciani, J.; Mudiyansele, K.; Xu, F.; Baber, A. E.; Evans, J.; Senanayake, S. D.; Stacchiola, D. J.; Liu, P.; Hrbek, J. et al. Highly Active Copper-Ceria and Copper-Ceria-Titania Catalysts for Methanol Synthesis from CO₂. *Science*. **2014**, *345*, 546–550.
- (6) Lunkenbein, T.; Schumann, J.; Behrens, M.; Schlögl, R.; Willinger, M. G. Formation of a ZnO Overlayer in Industrial Cu/ZnO/Al₂O₃ Catalysts Induced by Strong Metal – Support Interactions. *Angewandte. Angew. Chemie - Int. Ed.* **2015**, *54*, 4544–4548.
- (7) Vidal, A. B.; Feria, L.; Evans, J.; Takahashi, Y.; Liu, P.; Nakamura, K.; Illas, F.; Rodriguez, J. A. CO₂ Activation and Methanol Synthesis on Novel Au/TiC and Cu/TiC Catalysts. *J. Phys. Chem. Lett.* **2012**, *3*, 2275–2280.
- (8) Park, M. B.; Park, E. D.; Ahn, W.-S. Recent Progress in Direct Conversion of Methane to Methanol Over Copper-Exchanged Zeolites. *Front. Chem.* **2019**, *1*, 514.
- (9) Chen, F.; Zhang, P.; Zeng, Y.; Kosol, R.; Xiao, L.; Feng, X.; Li, J.; Liu, G.; Wu, J.; Yang, G. et al. Vapor-Phase Low-Temperature Methanol Synthesis from CO₂-Containing Syngas via Self-Catalysis of Methanol and Cu/ZnO Catalysts Prepared by Solid-State Method. *Appl. Catal. B Environ.* **2020**, *279*, 119382.
- (10) Lee, S. W.; Song, J. T.; Kim, J.; Oh, J.; Park, J. Y. Enhanced Catalytic Activity for CO Oxidation by the Metal–Oxide Perimeter of TiO₂ /Nanostructured Au Inverse Catalysts. *Nanoscale* **2018**, *10*, 3911–3917.
- (11) Wu, C.; Lin, L.; Liu, J.; Zhang, J.; Zhang, F.; Zhou, T.; Rui, N.; Yao, S.; Deng, Y.; Yang, F. et al. Inverse ZrO₂ /Cu as a Highly Efficient Methanol Synthesis Catalyst from CO₂ Hydrogenation. *Nat. Commun.* **2020**, *11*, 5767.
- (12) Li, Y.; Baumer, M.; Ivanova-shor, E. A.; Moskaleva, L. V. What Changes on the Inverse Catalyst? Insights from CO Oxidation on Au-Supported Ceria Nanoparticles Using Ab Initio Molecular Dynamics. *ACS Catal.* **2020**, *10*, 3164–3174.
- (13) Zhang, J.; Medlin, J. W. Catalyst Design Using an Inverse Strategy: From Mechanistic Studies on Inverted Model Catalysts to Applications of Oxide-Coated Metal Nanoparticles. *Surf. Sci. Rep.* **2018**, *73*, 117–152.
- (14) Fernández-García, M.; Martínez-Arias, A.; Hanson, J. C.; Rodriguez, J. A. Nanostructured Oxides in Chemistry: Characterization and Properties. *chem. rev.* **2004**, *104*, 4063–4104.
- (15) Netzer, F. P.; Allegretti, F.; Surnev, S. Low-Dimensional Oxide Nanostructures on Metals : Hybrid Systems with Novel Properties. *J. Vac. Sci. Technol. B* **2010**, *28*, 1.
- (16) Lunkenbein, T.; Schumann, J.; Behrens, M.; Schlögl, R.; Willinger, M. G. Formation of a ZnO Overlayer in Industrial Cu/ZnO/Al₂O₃ Catalysts Induced by Strong Metal-Support Interactions. *Angew. Chemie - Int. Ed.* **2015**, *54*, 4544–4548.
- (17) Kattel, S.; Ramírez, P. J.; Chen, J. G.; Rodriguez, J. A.; Liu, P. Active Sites for CO₂ Hydrogenation to Methanol on Cu/ZnO Catalysts. *Science*. **2017**, *355*, 1296–1299.
- (18) Rodriguez, J. A.; Ma, S.; Liu, P.; Hrbek, J.; Evans, J.; Pérez, M. Activity of CeO_x and TiO_x Nanoparticles Grown on Au(111) in the Water-Gas Shift Reaction. *Science*. **2007**, *318*, 1757–1760.
- (19) Palomino, R. M.; Gutiérrez, R. A.; Liu, Z.; Tenney, S.; Grinter, D. C.; Crumlin, E.; Waluyo, I.; Ramírez, P. J.; Rodriguez, J. A.; Senanayake, S. D. Inverse Catalysts for CO Oxidation: Enhanced Oxide-Metal Interactions in MgO/Au(111), CeO₂/Au(111), and TiO₂/Au(111). *ACS Sustain. Chem. Eng.* **2017**, *5*, 10783–10791.
- (20) Rodriguez, J. A.; Graciani, J.; Evans, J.; Park, J. B.; Yang, F.; Stacchiola, D.; Senanayake, S. D.; Ma, S.; Pérez, M.; Liu, P. et al. Water-Gas Shift Reaction on a Highly Active Inverse CeO_x /Cu(111) Catalyst: Unique Role of Ceria Nanoparticles. *Angew. Chemie Int. Ed.* **2009**, *48*, 8047–8050.

- (21) Rodríguez, J. A.; Liu, P.; Graciani, J.; Senanayake, S. D.; Grinter, D. C.; Stacchiola, D.; Hrbek, J.; Fernández-Sanz, J. Inverse Oxide/Metal Catalysts in Fundamental Studies and Practical Applications: A Perspective of Recent Developments. *J. Phys. Chem. Lett.* **2016**, *7*, 2627–2639.
- (22) Rodríguez, J. A.; Hrbek, J. Inverse Oxide/Metal Catalysts: A Versatile Approach for Activity Tests and Mechanistic Studies. *Surf. Sci.* **2010**, *604*, 241–244.
- (23) Axnanda, S.; Zhu, Z.; Zhou, W.; Mao, B.; Chang, R.; Rani, S.; Crumlin, E.; Somorjai, G.; Liu, Z. In Situ Characterizations of Nanostructured SnO_x/Pt(111) Surfaces Using Ambient-Pressure XPS (APXPS) and High-Pressure Scanning Tunneling Microscopy (HPSTM). *J. Phys. Chem. C* **2014**, *118*, 1935–1943.
- (24) Deng, X.; Lee, J.; Wang, C.; Matranga, C.; Aksoy, F.; Pennsylv, V.; States, U.; Box, P. O.; Park, S.; Pennsylv, V. et al. Reactivity Differences of Nanocrystals and Continuous Films of r-Fe₂O₃ on Au (111) Studied with In Situ X-Ray Photoelectron Spectroscopy. *J. Phys. Chem. C* **2010**, *114*, 22619–22623.
- (25) Bai, H.; Guo, H.; Wang, J.; Dong, Y.; Liu, B.; Guo, F.; Chen, D.; Zhang, R.; Zheng, Y. Hydrogen Gas Sensor Based on SnO₂ Nanospheres Modified with Sb₂O₃ Prepared by One-Step Solvothermal Route. *Sensors Actuators, B Chem.* **2021**, *331*, 129441.
- (26) Choi, P. G.; Izu, N.; Shirahata, N.; Masuda, Y. Fabrication and H₂-Sensing Properties of SnO₂ Nanosheet Gas Sensors. *ACS Omega* **2018**, *3*, 14592–14596.
- (27) Fedorenko, G.; Oleksenko, L.; Maksymovych, N.; Skolyar, G.; Ripko, O. Semiconductor Gas Sensors Based on Pd/SnO₂ Nanomaterials for Methane Detection in Air. *Nanoscale Res. Lett.* **2017**, *12*, 329.
- (28) Batzill, M. Surface Science Studies of Gas Sensing Materials: SnO₂. *Sensors* **2006**, *6*, 1345–1366.
- (29) Bai, S.; Xu, Y.; Cao, K.; Huang, X. Selective Ethanol Oxidation Reaction at the Rh–SnO₂ Interface. *Adv. Mater.* **2021**, *33*, 2005767.
- (30) Axnanda, S.; Zhou, W. P.; White, M. G. CO Oxidation on Nanostructured SnO_x/Pt(111) Surfaces: Unique Properties of Reduced SnO X. *Phys. Chem. Chem. Phys.* **2012**, *14*, 10207–10214.
- (31) Narayanaru, S.; Anilkumar, G. M.; Ito, M.; Tamaki, T.; Yamaguchi, T. An Enhanced Electrochemical CO₂ reduction Reaction on the SnO: X-PdO Surface of SnPd Nanoparticles Decorated on N-Doped Carbon Fibers. *Catal. Sci. Technol.* **2021**, *11*, 143–151.
- (32) Guharoy, U.; Le Saché, E.; Cai, Q.; Reina, T. R.; Gu, S. Understanding the Role of Ni-Sn Interaction to Design Highly Effective CO₂ Conversion Catalysts for Dry Reforming of Methane. *J. CO₂ Util.* **2018**, *27*, 1–10.
- (33) Zhang, L.; Hu, Y.; Xu, W.; Huang, C.; Su, Y.; Tian, M.; Zhu, Y.; Gong, H.; Wang, X. Anti-Coke BaFe_{1-x}Sn_xO_{3-δ} Oxygen Carriers for Enhanced Syngas Production via Chemical Looping Partial Oxidation of Methane. *energy fuels* **2020**, *34*, 6991–6998.
- (34) Kim, Y.; Kim, J.; Kim, H. W.; Kim, T.; Kim, H. J.; Chang, H.; Park, M. B.; Chae, H. Sulfated Tin Oxide as Highly Selective Catalyst for the Chlorination of Methane to Methyl Chloride. *ACS Catal.* **2019**, *9*, 9398–9410.
- (35) Kang, J.; Rui, N.; Huang, E.; Tian, Y.; Mahapatra, M.; Rosales, R.; Orozco, I.; Shi, R.; Senanayake, S. D.; Liu, P. et al. Surface Characterization and Methane Activation on SnO_x/Cu₂O/Cu(111) Inverse Oxide/Metal Catalysts †. *Phys. Chem. Chem. Phys.* **2021**, *23*, 17186.
- (36) Hanke, F.; Björk, J. Structure and Local Reactivity of the Au(111) Surface Reconstruction. *Phys. Rev. B* **2013**, *87*, 235422.
- (37) McClure, S. M.; Kim, T. S.; Stiehl, J. D.; Tanaka, P. L.; Mullins, C. B. Adsorption and Reaction of Nitric Oxide with Atomic Oxygen Covered Au(111). *J. Phys. Chem. B* **2004**, *108*, 17952–17958.
- (38) Mahapatra, M.; Kang, J.; Ramírez, P. J.; Hamlyn, R.; Rui, N.; Liu, Z.; Orozco, I.; Senanayake, S. D.; Rodríguez, J. J. Growth, Structure, and Catalytic Properties of ZnO_x Grown on CuO_x/Cu(111) Surfaces. *J. Phys. Chem. C* **2018**, *122*, 53.

- (39) Mahapatra, M.; Gutiérrez, R. A.; Kang, J.; Rui, N.; Hamlyn, R.; Liu, Z.; Orozco, I.; Ramírez, P. J.; Senanayake, S. D.; Rodriguez, J. A. The Behavior of Inverse Oxide/Metal Catalysts: CO Oxidation and Water-Gas Shift Reactions over ZnO/Cu(111) Surfaces. *Surf. Sci.* **2019**, *681*, 116–121.
- (40) Sadhukhan, P.; Pandey, D.; Singh, V. K.; Sarkar, S.; Rai, A.; Bhattacharya, K.; Chakrabarti, A.; Roy Barman, S. Electronic Structure and Morphology of Thin Surface Alloy Layers Formed by Deposition of Sn on Au(111). *Appl. Surf. Sci.* **2020**, *506*, 144606.
- (41) Barthès, M. G.; Pariset, C. A Low Energy Electron Diffraction-Auger Electron Spectroscopy Study of Alloy Formation during the Adsorption of Tin on (100) and (111) Au. *Thin Solid Films* **1981**, *77*, 305–312.
- (42) Maniraj, M.; Jungkenn, D.; Shi, W.; Emmerich, S.; Lyu, L.; Kollamana, J.; Wei, Z.; Yan, B.; Cinchetti, M.; Mathias, S. et al. Structure and Electronic Properties of the (3 × 3)R30 SnAu₂/Au(111) Surface Alloy. *Phys. Rev. B* **2018**, *98*, 205419.
- (43) Meier, L. A.; Castellani, N. J. Theoretical Study of Sn Adsorbed on the Au(111) Surface. *Comput. Mater. Sci.* **2017**, *127*, 48–59.
- (44) Zhang, Y.; Slavin, A. J. Adsorption of Metallic Tin on the Au(111) Surface. *Cit. J. Vac. Sci. Technol. A* **1991**, *9*, 1784.
- (45) Yamada, T.; Miura, K.; Kajihara, M.; Kurokawa, N.; Sakamoto, K. Kinetics of Reactive Diffusion between Au and Sn during Annealing at Solid-State Temperatures. *Mater. Sci. Eng. A* **2005**, *390*, 118–126.
- (46) Luo, Y. *Bond Dissociation Energies*; CRC Press: Boca Raton, FL, 2007.
- (47) Chado, I.; Scheurer, F.; Bucher, J. P. Absence of Ferromagnetic Order in Ultrathin Rh Deposits Grown under Various Conditions on Gold. *Phys. Rev. B* **2001**, *64*, 094410.
- (48) Fonin, M.; Dedkov, Y. S.; Rüdiger, U.; Güntherodt, G. Growth and Structure of Mn on Au(111) at Room Temperature. *Surf. Sci.* **2003**, *529*, 1–6.
- (49) Wang, Z. T.; Darby, M. T.; Therrien, A. J.; El-Soda, M.; Michaelides, A.; Stamatakis, M.; Sykes, E. C. H. Preparation, Structure, and Surface Chemistry of Ni-Au Single Atom Alloys. *J. Phys. Chem. C* **2016**, *120*, 13574–13580.
- (50) Nouvertne, F.; May, U.; Bamming, M.; Rampe, A.; Korte, U.; Guntherodt, G. Atomic Exchange Processes and Bimodal Initial Growth of Co/Cu(001). *Phys. Rev. B* **1999**, *60*, 14382–14386.
- (51) Vitos, L.; Ruban, A. V.; Skriver, H. L.; Kollár, J. The Surface Energy of Metals. *Surf. Sci.* **1998**, *411*, 186–202.
- (52) Taylor, J. A.; Lancaster, G. M.; Rabalais, J. W. Chemical Reactions of N₂⁺ Ion Beams with Group IV Elements and Their Oxides. *J. Electron Spectros. Relat. Phenomena* **1978**, *13*, 435–444.
- (53) Willemen, H.; Van De Vondel, D. F.; Van Der Kelen, G. P. An ESCA Study of Tin Compounds. *Inorganica Chim. Acta* **1979**, *34*, 175–180.
- (54) Zhou, W.; Axnanda, S.; White, M. G.; Adzic, R. R.; Hrbek, J. Enhancement in Ethanol Electrooxidation by SnO_x Nanoislands Grown on Pt (111): Effect of Metal Oxide À Metal Interface Sites. *J. Phys. Chem. C* **2011**, *115*, 16467–16473.
- (55) Axnanda, S.; Zhou, W. P.; White, M. G. CO Oxidation on Nanostructured SnO_x/Pt(111) Surfaces: Unique Properties of Reduced SnO_x. *Phys. Chem. Chem. Phys.* **2012**, *14*, 10207–10214.
- (56) Yan, J. W.; Xie, Z. X.; Cao, Z. X.; Zhou, C. J.; Kang, J. Y.; Mao, B. W. Formation and STM Tip-Induced Reduction of Ultra Thin SnO Film on Au(111). *Chem. Phys. Lett.* **2003**, *373*, 575–579.
- (57) Chan, S. I.; Yu, S. S. F. Controlled Oxidation of Hydrocarbons by the Membrane-Bound Methane Monooxygenase: The Case for a Tricopper Cluster. *Acc. Chem. Res.* **2008**, *41*, 969–979.

- (58) Wang, V. C. C.; Maji, S.; Chen, P. P. Y.; Lee, H. K.; Yu, S. S. F.; Chan, S. I. Alkane Oxidation: Methane Monooxygenases, Related Enzymes, and Their Biomimetics. *Chem. Rev.* **2017**, *117*, 8574–8621.
- (59) Paolucci, V.; D'Olimpio, G.; Kuo, C. N.; Lue, C. S.; Boukhvalov, D. W.; Cantalini, C.; Politano, A. Self-Assembled SnO₂/SnSe₂ Heterostructures: A Suitable Platform for Ultrasensitive NO₂ and H₂ Sensing. *ACS Appl. Mater. Interfaces* **2020**, *12*, 34362–34369.
- (60) Palomino, R. M.; Ramírez, P. J.; Liu, Z.; Hamlyn, R.; Waluyo, I.; Mahapatra, M.; Orozco, I.; Hunt, A.; Simonovis, J. P.; Senanayake, S. D.; et al. Hydrogenation of CO₂ on ZnO/Cu(100) and ZnO/Cu(111) Catalysts: Role of Copper Structure and Metal–Oxide Interface in Methanol Synthesis. *J. Phys. Chem. B* **2018**, *122*, 794–800.
- (61) Eren, B.; Weatherup, R. S.; Liakakos, N.; Somorjai, G. A.; Salmeron, M. Dissociative Carbon Dioxide Adsorption and Morphological Changes on Cu (100) and Cu (111) at Ambient Pressures. *J. Am. Chem. Soc.* **2016**, *138*, 8207–8211.
- (62) Graciani, J.; Vidal, A.B.; Rodriguez, J.A.; Sanz, J.F. Unraveling the Nature of the Oxide–Metal Interaction in Ceria-Based Noble Metal Inverse Catalysts, *J. Phys. Chem. C*, 2014, *118*, 46, 26931–26938



TOC Graphic